# General Top-Down Ion Exchange Process for the Growth of Epitaxial Chalcogenide Thin Films and Devices

Chuan Xia,[†] Peng Li,[†] Jun Li, Qiu Jiang, Xixiang Zhang,* and Husam N. Alshareef*[ID]

Materials Science and Engineering, King Abdullah University of Science and Technology (KAUST), Thuwal 23955-6900, Saudi Arabia

Ⓢ *Supporting Information*

**ABSTRACT:** We demonstrate a versatile top-down ion exchange process, done at ambient temperature, to form epitaxial chalcogenide films and devices, with nanometer scale thickness control. To demonstrate the versatility of our process we have synthesized (1) epitaxial chalcogenide metallic and semiconducting films and (2) free-standing chalcogenide films and (3) completed *in situ* formation of atomically sharp heterojunctions by selective ion exchange. Epitaxial $NiCo_2S_4$ thin films prepared by our process show 115 times higher mobility than $NiCo_2S_4$ pellets (23 vs 0.2 $cm^2 V^{-1} s^{-1}$) prepared by previous reports. By controlling the ion exchange process time, we made free-standing epitaxial films of $NiCo_2S_4$ and



transferred them onto different substrates. We also demonstrate *in situ* formation of atomically sharp, lateral Schottky diodes based on $NiCo_2O_4/NiCo_2S_4$ heterojunction, using a single ion exchange step. Additionally, we show that our approach can be easily extended to other chalcogenide semiconductors. Specifically, we used our process to prepare $Cu_{1.8}S$ thin films with mobility that matches single crystal $Cu_{1.8}S$ (25 $cm^2 V^{-1} s^{-1}$), which is ca. 28 times higher than the previously reported $Cu_{1.8}S$ thin film mobility (0.58 $cm^2 V^{-1} s^{-1}$), thus demonstrating the universal nature of our process. This is the first report in which chalcogenide thin films retain the epitaxial nature of the precursor oxide films, an approach that will be useful in many applications.
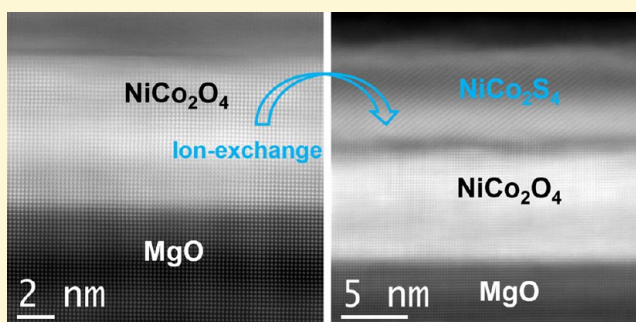
## 1. INTRODUCTION

Thin transition metal chalcogenide films are of particular interest for the fabrication of optoelectronics,[1,2] photovoltaic cells,[3,4] thermoelectrics,[5,6] sensors,[7,8] etc. While several bottom-up solution approaches[9−13] have been used to grow chalcogenide films, they often result in rough surface morphology and high defect density, with film thickness of tens of microns.[14] The poor properties associated with defect-rich thick films have recently shifted the research effort to atomic crystals and ultrathin epitaxial films.[15,16] Direct heteroepitaxy of chalcogenides thin films on cheap, commercially available oxide substrates is very difficult, considering the large lattice parameter mismatch and/or thermal-expansion coefficient between the film and substrate. Meanwhile, traditional bottom-up solution routes also cannot be controlled with nanoscale precision. Therefore, even with the abundance of chemical synthetic routes for transition metal chalcogenide thin film synthesis, obtaining high-quality epitaxial chalcogenide ultrathin films over large substrates is still a considerable challenge and has not been realized to date.

Here, we develop a thickness controllable, area selective top-down solution approach to realize epitaxial chalcogenide films and devices. Specifically, we have developed a process for $NiCo_2S_4$ thin films and freestanding quasi-single-crystal $NiCo_2S_4$ thin films under ambient conditions. Moreover, we fabricated in situ oxide-chalcogenide lateral $NiCo_2O_4/NiCo_2S_4$

Schottky diodes and $Cu_{1.8}S$ films with single-crystal-like performance. Our analysis reveals that this top-down route offers the capability to achieve an atomically sharp transition at the junction's interface. The procedures for forming $NiCo_2S_4$ epitaxial thin film comprises two steps, where epitaxial $NiCo_2O_4$ is first grown on single crystal substrate (e.g., MgO) as template, followed by the top-down solution anion-exchange reaction to induce epitaxy of $NiCo_2S_4$ which was schematically illustrated in Scheme 1. The epitaxial $NiCo_2O_4$ films also mitigate the lattice mismatch between $NiCo_2S_4$ and MgO substrate, in case of direct chalcogenide film growth on MgO. The extent of the ion exchange process can be changed to control the thickness of the $NiCo_2O_4$ that is converted to $NiCo_2S_4$. If the ion exchange reaction is carried out long enough, the entire layer of $NiCo_2O_4$ is converted to $NiCo_2S_4$, and the newly formed $NiCo_2S_4$ thin film can be peeled off from the MgO substrate easily to form a freestanding quasi-single-crystal thin film. These freestanding chalcogenide films can be transferred onto other substrates to make nanodevices coupled with other atomic crystals. In fact, this is the first report in which the chalcogenide thin films can retain the epitaxial nature of their precursor oxide films. This is analogous to ionic

**Scheme 1. Schematic of the Top-down Process We Developed for the Formation of Epitaxial of NiCo$_2$S$_4$ (AB$_2$S$_4$) Thin Films from the NiCo$_2$O$_4$ (AB$_2$O$_4$) Template[a]**
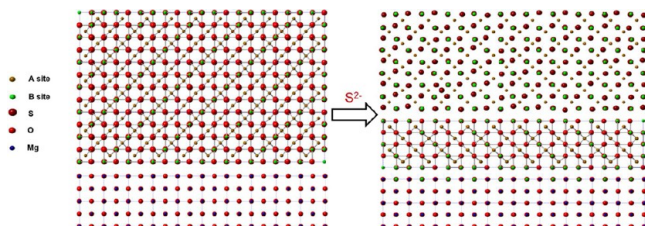


[a]Single crystal MgO substrate was used in this study.

nanocrystals, but not thin films, which were recently shown to preserve both the anion and cation sublattice of the precursor nanocrystals during solution ion-exchange process.[17−21] We believe that this strategy can be extended to fabricate various kinds of high-quality transition metal chalcogenide thin films and corresponding heterojunctions, for example, ZnS, Ag$_2$S, Cu$_{1.8}$S, CdS, CoS, MnS, CdSe, Cu$_2$Se, etc.

## 2. EXPERIMENTAL SECTION

**2.1. Epitaxial NiCo$_2$O$_4$ Thin Film Synthesis.** The epitaxial NiCo$_2$O$_4$ films were grown by pulsed laser deposition. The NiCo$_2$O$_4$ films were fabricated on single crystal substrate (001) MgO at 350 °C under 50 mTorr of O$_2$. The NiCo$_2$O$_4$ target was synthesized by the hydrothermal method (ref 25) and was ablated by KrF excimer laser ($\lambda$ = 248 nm) at 10 Hz with a fluence of 2.8 J cm$^{-2}$. The thickness of epitaxial NiCo$_2$O$_4$ films ranged from 15 to 20 nm. The very small lattice mismatch (NiCo$_2$O$_4$: 8.11 Å, MgO: 4.2 Å) helps to achieve epitaxy of NiCo$_2$O$_4$ (001) on MgO (001).

**2.2. Epitaxial Cu$_2$O Thin Film Synthesis.** The epitaxial Cu$_2$O films were grown by reactive sputtering. The (011) oriented epitaxial Cu$_2$O films were prepared on MgO (001) at 700 °C under 1 mTorr of O$_2$ and 6 mTorr of Ar. A rotation of 45° for the Cu$_2$O (001) plane with respect to MgO (001) is expected because the distance between the nearest neighboring Cu atoms is $\sqrt{2}/2 \times 4.217$ Å (lattice constant of Cu$_2$O: 4.217 Å). The thickness of Cu$_2$O was maintained at 300 nm.

**2.3. Epitaxial and Freestanding NiCo$_2$S$_4$ Thin Film Synthesis.** The as-prepared epitaxial thin NiCo$_2$O$_4$ films (∼15 nm) in 0.1 M NaHS aqueous solution (10 mL) were placed in a reaction vessel at room-temperature for 12 h to prepare ca. 7 nm NiCo$_2$S$_4$ thin film. In order to obtain ∼2 nm thin NiCo$_2$S$_4$ film, the reaction time was decreased to 2 h. To obtain pristine "fully converted" thin NiCo$_2$S$_4$ film, the reaction time was increased to 7 days. All the room-temperature processed films were annealed at 300 °C in Ar for 1 h. To prepare freestanding thin NiCo$_2$S$_4$ film, 40 mL of 0.05 M Na$_2$S
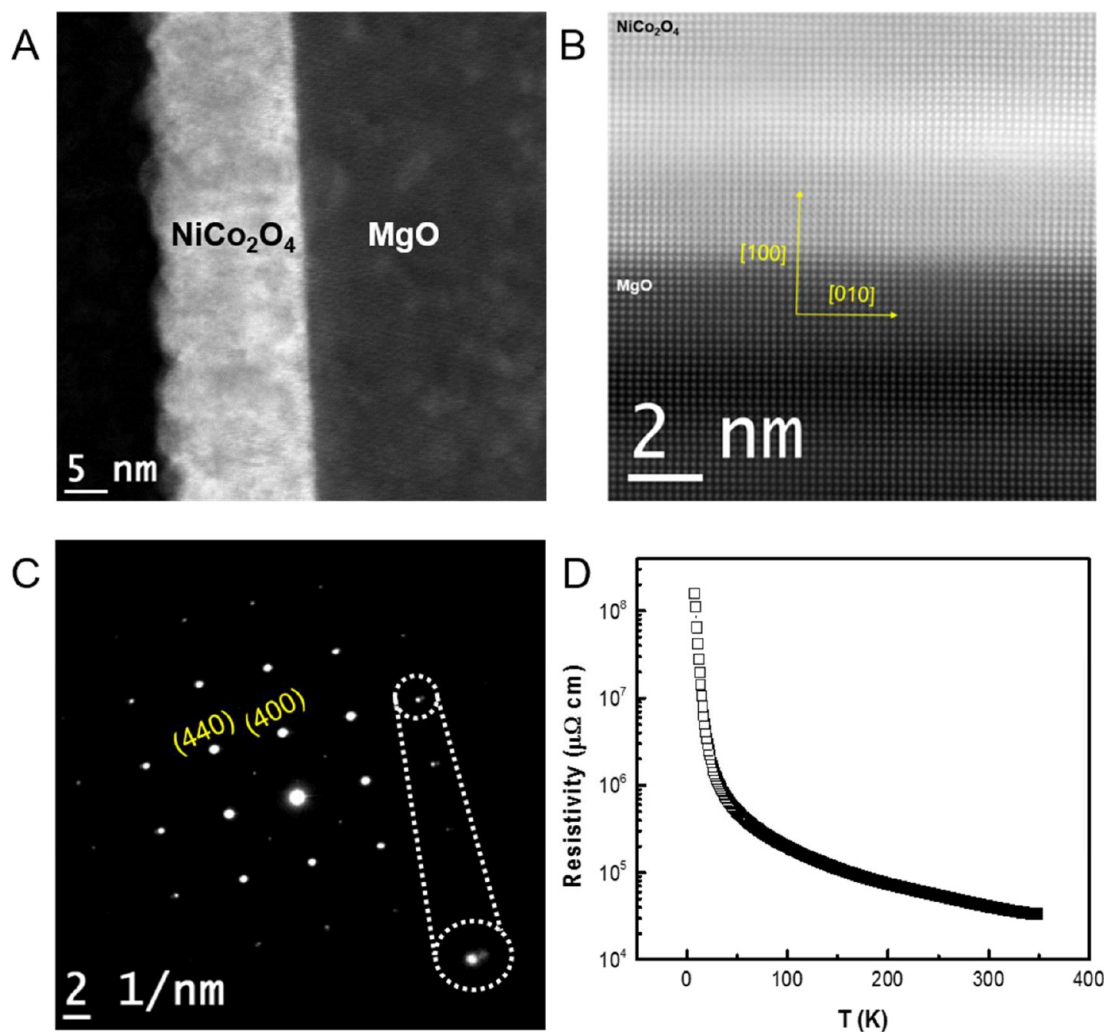


**Figure 1.** Characterization of epitaxial NiCo$_2$O$_4$ thin films on MgO substrate. (A, B) HAADF-STEM images of NiCo$_2$O$_4$/MgO sample and (C) corresponding SAED pattern. (D) Resistivity of NiCo$_2$O$_4$ as a function of temperature.
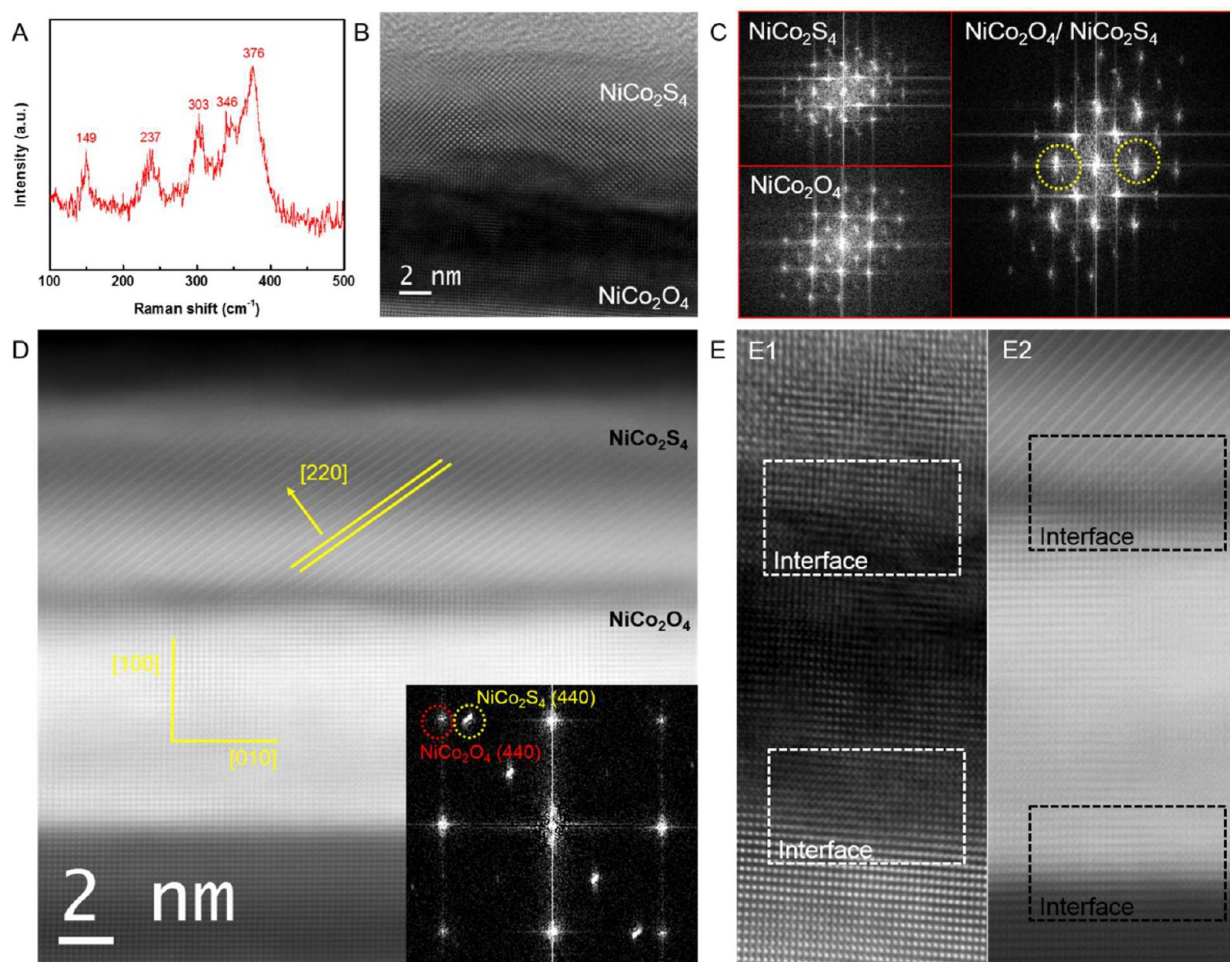
**Figure 2.** Characterization of epitaxial NiCo₂S₄ thin films synthesized by top-down ion exchange. (A) Raman spectra of annealed NiCo₂S₄ measured in argon atmosphere. (B) The bright-field TEM of annealed NiCo₂S₄/NiCo₂O₄ interface and (C) corresponding FFT images. (D) HAADF-STEM image of annealed bilayer NiCo₂S₄/NiCo₂O₄ thin film on MgO substrate. The inset image shows the FFT around the interface region. (E) High-resolution TEM images of NiCo₂S₄/NiCo₂O₄/MgO sample, showing atomically sharp transition across the interface region. E1 and E2 are bright-field TEM and HAADF-STEM images of NiCo₂S₄/NiCo₂O₄/MgO, respectively.

aqueous solution was transferred into a Teflon-lined autoclave with a piece of as-prepared epitaxial thin NiCo₂O₄ film immersed into the solution and kept at 120 °C for 4 h. After cooling down to room temperature, the as-obtained free-standing films were transferred onto Si/SiO₂ substrate for electrical transport studies.

**2.4. Quasi-Single-Crystal Cu₁.₈S Thin Film Synthesis.** Approximately 500 μL of 0.1 M Na₂S aqueous solution was added into 10 mL of methanol. Next, this solution was cooled in an ice-bath for 10 min. Afterward, one piece of as-synthesized epitaxial Cu₂O film was immersed into this solution and kept in an ice-bath for 1 h. The as-obtained copper sulfide films were annealed at 300 °C in Ar for 1 h.

**2.5. Characterization.** X-ray diffraction (XRD) spectra were collected by a Bruker diffractometer (D8 Advance) with Cu Kα radiation, λ = 1.5406 Å. The XRD φ scan was conducted on Bruker D8 discover. The bright-field TEM images were collected from Titan 80−300 kV (ST) TEM, FEI. Further, the spherical-aberration-corrected TEM images were collected from FEI Probe Corrected Titan3 80−300 S/TEM. Energy-dispersive spectroscopy (EDS) elemental mapping analysis was performed on the same instrument in scanning TEM (STEM) mode. Pristine "fully converted" NiCo₂S₄ thin films were studied by confocal Raman spectroscopy for Raman studies to exclude the signals from NiCo₂O₄. Raman experiments were carried out on a Hariba LAB RAM HR spectrometer.

**2.6. Device Fabrication.** The freestanding NiCo₂S₄ thin films were transferred onto Si/SiO₂ (280 nm) wafers first. Afterward, the Ti (10 nm)/Au (100 nm) electrodes for transport tests were fabricated on the high quality samples (flat, large) using standard e-beam lithography (EBL) and e-beam evaporation. To prepare lateral NiCo₂O₄/NiCo₂S₄ heterojunctions, the NiCo₂O₄/MgO samples were first patterned using photoresist for area selective exposure. Then, the patterned samples were immersed into aqueous sulfides solution for 6 h. After anion-exchange, the resist was then stripped by soaking the samples in acetone. Next, the samples were annealed in Ar atmosphere for 1 h.

**2.7. Measurement of Physical Properties.** The electrical transport properties were measured using a physical property measurement system (Dynacool, Quantum Design). The transport properties of as-made Schottky diode (NiCo₂O₄/NiCo₂S₄) were analyzed by Keithley 4200 semiconductor characterization system.

## 3. RESULTS AND DISCUSSION

**3.1. Epitaxial Growth of Spinel NiCo₂O₄ on MgO (100).** The first step in this process is to develop a route to deposit epitaxial oxide films. Here, we have deposited spinel NiCo₂O₄ epitaxial thin films on MgO substrates using pulsed laser deposition, but other methods can be used (see details in Experimental Section). The spinel NiCo₂O₄ crystal is composed of a face-centered cubic O²⁻ sublattice, where Ni cations occupy the octahedral sites, while Co cations are evenly distributed between octahedral and tetrahedral sites.[22] Figure S1 shows the θ−2θ X-ray diffraction (XRD) pattern of a
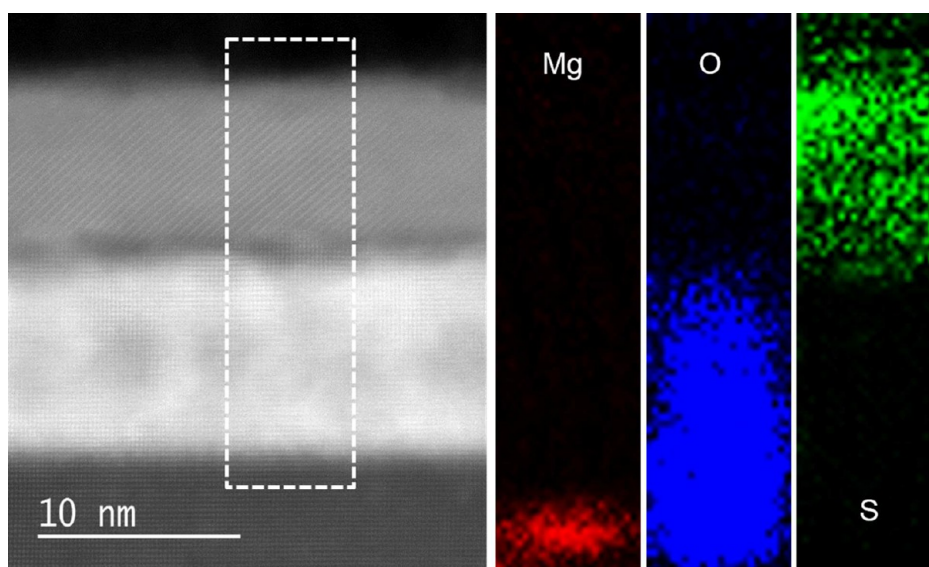
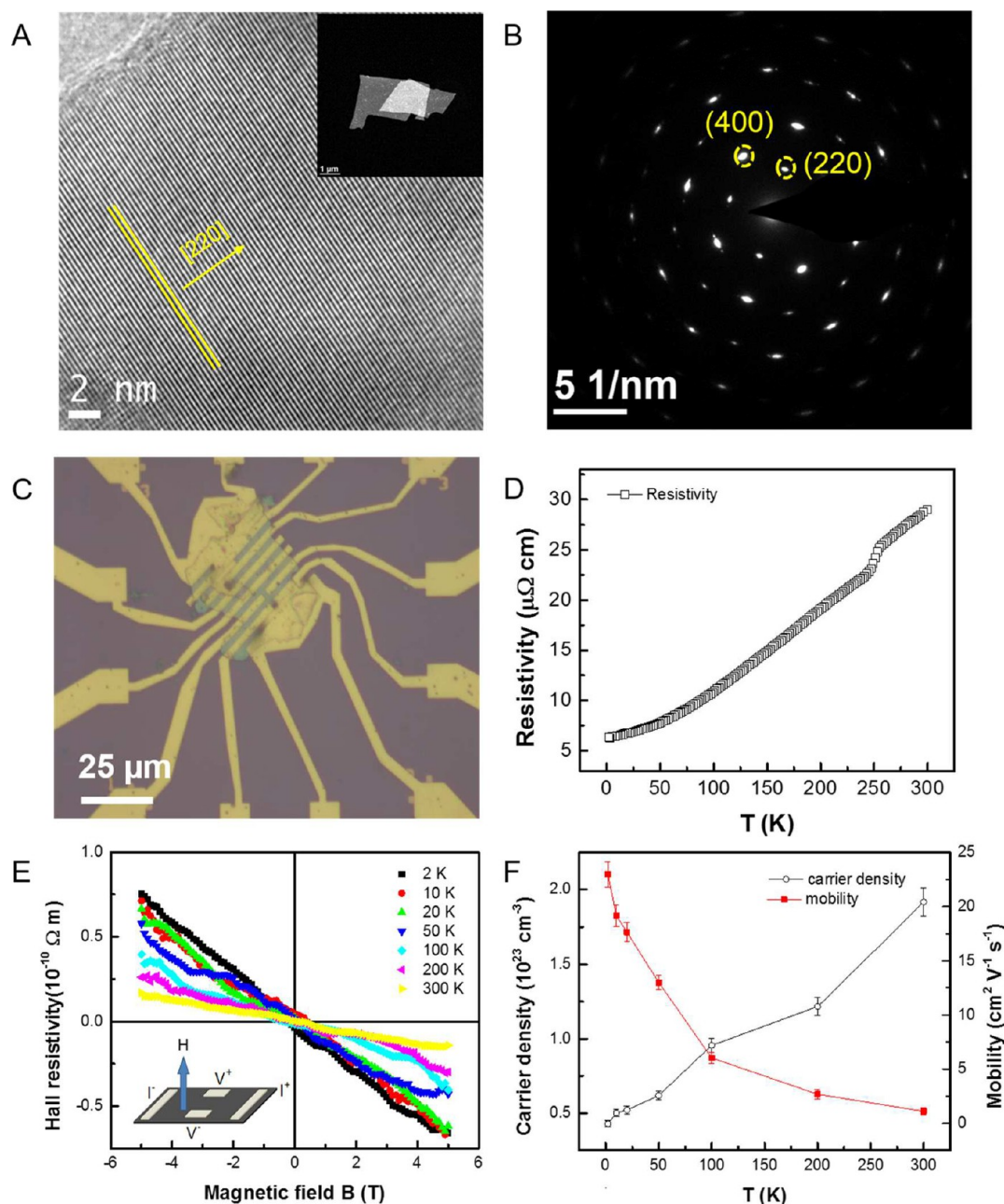**Figure 3.** Characterization of vertical $NiCo_2S_4/NiCo_2O_4/MgO$ heterojunction. STEM-EDS elemental mapping of Mg, O, and S from Ar annealed $NiCo_2S_4/NiCo_2O_4/MgO$ sample.

$NiCo_2O_4/MgO$ films. Only $NiCo_2O_4$ (400) diffraction peaks can be observed from the film, which indicates that the as-prepared thin film is preferentially oriented along the $[100]$ direction. To gain more insight into the structure of the as-prepared thin films, we conducted spherical-aberration corrected high-angle annular dark-field (HAADF) scanning transmission electron microscopy (STEM) studies. The HAADF STEM is sensitive to the atomic number and can clearly differentiate composition changes at a sharp interface.[23] Figure 1a reveals the successful growth of $NiCo_2O_4$ thin film on MgO (100), with a thickness of around 15 nm and relativity smooth surface. The high-resolution HAADF-STEM image (Figure 1b) is focused on $NiCo_2O_4/MgO$ interface region, which shows perfect epitaxy of $NiCo_2O_4$ on the MgO substrate and a distinguishable interface. The corresponding selected-area electron diffraction (SAED) analysis around the interface region confirms the existence of a high-quality epitaxial thin film, as shown in Figure 1c. A magnified view of the diffraction pattern reveals that each diffraction spot consists of a pair of diffraction peaks (see inset in Figure 1c), confirming the perfect growth of $NiCo_2O_4$ thin film on the substrate, with a small contraction of the $NiCo_2O_4$ lattice (0.811 nm) compared to MgO (0.420 nm).[15] It should be noted that this epitaxial relationship is observed over the entire 1 cm × 1 cm MgO substrate. In fact, we performed the TEM analysis on various parts of the crystal and confirmed that the observed epitaxy covers the entire substrate. Figure 1d displays the resistivity–temperature (RT) curve of as-made $NiCo_2O_4$ thin film from 2 to 300 K. It is clear that the epitaxial $NiCo_2O_4$ film shows semiconducting behavior, which is consistent with previous reports.[24,25] Based on the above discussion, we believe that good quality epitaxial $NiCo_2O_4$ thin films have been successfully deposited.

**3.2. Top-down Anion-Exchange Process To Form Epitaxial $NiCo_2S_4$ Thin Films.** Our objective was to determine if we can preserve the epitaxial relation while converting the epitaxial films $NiCo_2O_4$, by ion exchange, to $NiCo_2S_4$. To carry out the ion exchange process, our $NiCo_2O_4$ thin films were first immersed into a sulfide aqueous solution at room temperature, followed by Ar atmosphere annealing at 300

°C. By controlling the ion exchange process time and/or temperature, we could partially or completely convert $NiCo_2O_4$ to $NiCo_2S_4$. In fact, our ion exchange process was used to make chalcogenide films as thin as 2 nm or as thick as the entire $NiCo_2O_4$ film we started with. To illustrate this concept, we show the results where only the top 7 nm of the starting $NiCo_2O_4$ film was converted to $NiCo_2S_4$, thus creating a vertical $NiCo_2S_4/NiCo_2O_4$ heterojunction. Figure S2a displays the cross-section TEM images of heterojunction formed by partial ion exchange. The close-up TEM images (Figure S2b) of the $NiCo_2O_4$ film demonstrate that the topmost layer with a thickness of ca. 7 nm has been converted to a new phase after ion exchange at room temperature. In this new layer, the Co and Ni sublattices retain their position and epitaxial relationship with the MgO substrate, but the $O^{2-}/S^{2-}$ sublattice is disordered, as illustrated in the schematic shown in the Scheme S1. The energy-dispersive spectroscopy (EDS) analysis (Figure S2d) shows the composition of the topmost layer was nickel, cobalt, and sulfur, suggesting the formation of the desired $NiCo_2S_4$ thin film. The unconverted $NiCo_2O_4$ layer retains its crystallinity (Figure S2c), indicating that our top-down ion exchange process can control thickness at the nanoscale, without degrading the unconverted region. The crystal structure, composition, and growth mechanism of the converted $NiCo_2S_4$ layer were studied immediately after the ion exchange process and after annealing at 300 °C in Ar for 1 h. Confocal Raman spectroscopy tests were performed on freshly converted $NiCo_2S_4$ thin films in Ar atmosphere to exclude any laser-induced oxidation of $NiCo_2S_4$ in air (see preparation details in Experimental Section).[26] The Raman data in Figure 2a strongly support the formation of crystallized $NiCo_2S_4$, as evidenced by the sharp peaks at 149, 237, 303, 346, and 376 $cm^{-1}$ which are in good agreement, respectively, with previous experimental and theoretical Raman features of the $T_{2g,3}$, $E_g$, $T_{2g,2}$, $T_{2g,1}$, and $A_{1g}$ of $NiCo_2S_4$.[26] Further, the cross-section TEM and HAADF-STEM images of crystallized $NiCo_2S_4$ are shown in Figure 2. The bright-field TEM image (Figure 2b) of the $NiCo_2S_4/NiCo_2S_4$ interface region clearly demonstrates a typical spinel-on-spinel epitaxial feature, as well as an atomically sharp transition across the junction. The

**Figure 4.** Characterization of electrical transport properties of freestanding $NiCo_2S_4$ thin film. (A) High-resolution TEM and HAADF STEM images of freestanding $NiCo_2S_4$ thin film with (B) corresponding SAED pattern. (C) Optical microscope image of a sample nanodevice based on $NiCo_2S_4$ thin film. (D) Resistivity of $NiCo_2S_4$ as a function of temperature. (E) Magnetic field dependent Hall resistivity of $NiCo_2S_4$ at different temperatures. The inset gives the Hall measurement configuration. (F) Calculated carrier density (black circles) and mobility (red squares) as a function of temperature.

corresponding fast Fourier transformed (FFT) images (Figure 2c) also confirm the epitaxy of the $NiCo_2S_4$ thin films obtained from $NiCo_2O_4$. We further examined the interface of the $NiCo_2S_4$/$NiCo_2O_4$ junction using spherical-aberration corrected HAADF-STEM. As shown in Figure 2d, the bilayer heterojunction on the MgO substrate was observed with distinct MgO/$NiCo_2O_4$ and $NiCo_2O_4$/$NiCo_2S_4$ transition regions. Figure 2d shows resolved-lattice fringes with spacing of ca. 0.332 nm in the topmost layer, corresponding to the thiospinel $NiCo_2S_4$ (220) crystal plane. In principle, the [220] direction of solution-processed epitaxial $NiCo_2S_4$ thin film should be parallel with $NiCo_2O_4$ [220] if the $NiCo_2S_4$ film has perfect epitaxy with $NiCo_2O_4$, implying a 45° angle exists

between the $NiCo_2O_4$ [040] direction and the $NiCo_2S_4$ [220] direction. Interestingly, our detailed analysis shows that the angle between the $NiCo_2O_4$ [040] direction and the $NiCo_2S_4$ [220] direction in the 7 nm converted layer is actually 39°, meaning that the [100] direction of the $NiCo_2S_4$ thin film is 6° angled to the MgO and $NiCo_2O_4$ [100] direction. This is the reason why we could not observe the apparent $NiCo_2S_4$ lattice pattern when the electron beam was parallel to the MgO {100} zone axis (Figure 2d). We believe that this shift of the $NiCo_2S_4$ {100} zone axis results from the large lattice parameter mismatch between $NiCo_2S_4$ and $NiCo_2O_4$. The lattice constant of $NiCo_2S_4$ is 0.938 nm, whereas that of $NiCo_2O_4$ is 0.811 nm. This is 15.6% mismatch of lattice constant, which can lead to a
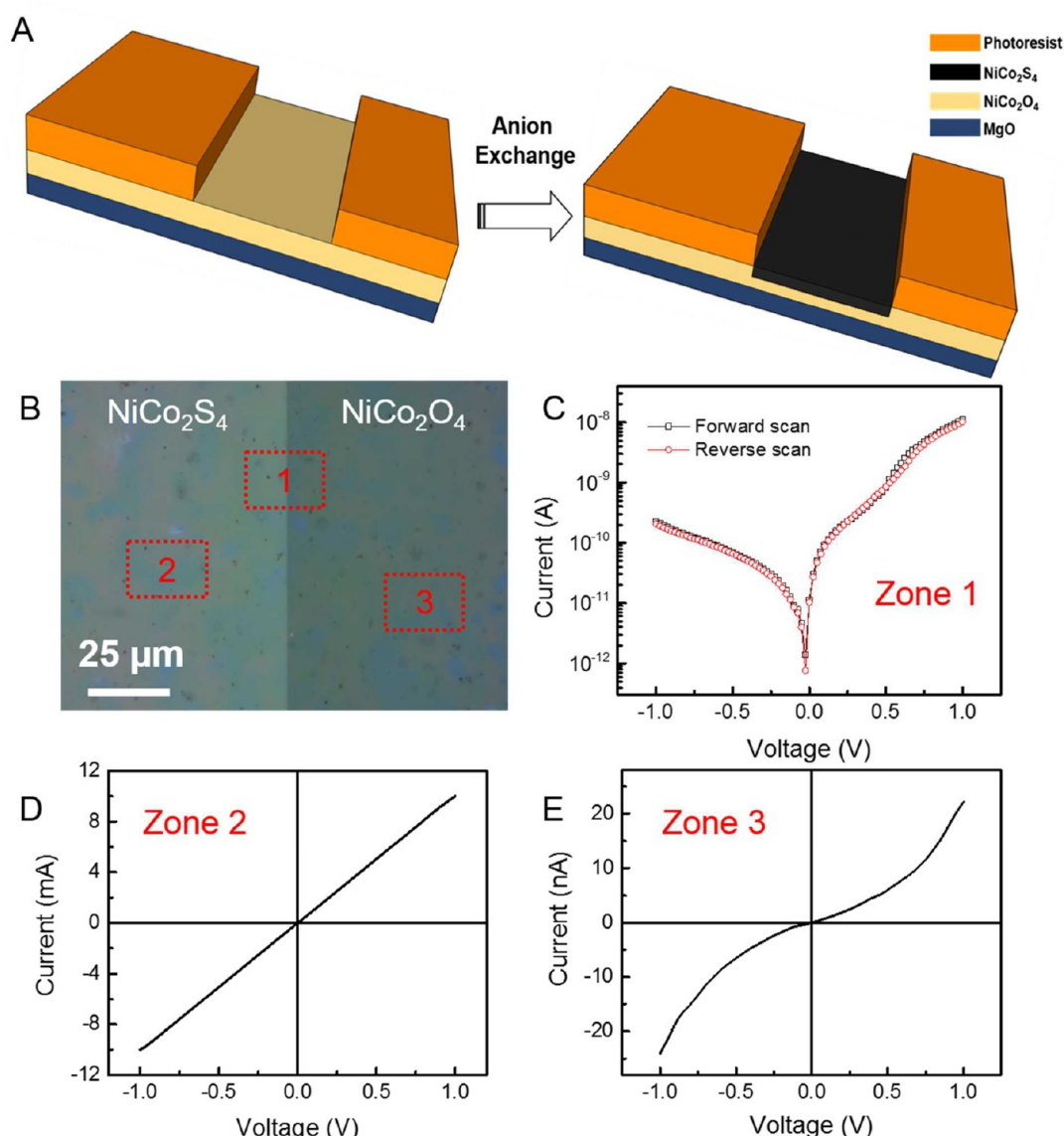
**Figure 5.** Characterization of lateral $NiCo_2S_4/NiCo_2O_4$ Schottky diode. (A) 3D schematic of the structure and process used to make the lateral Schottky diodes. (B) Optical microscope image of a representative diode. $I−V$ curves collected from (C) zone 1, (D) zone 2, and (E) zone 3 in Figure 4b, respectively.

strong strain in the room-temperature prepared $NiCo_2S_4$ thin film. During the annealing process, the undesirable strain in the films is gradually released, resulting in a distortion of the topmost $NiCo_2S_4$ layer. This process is illustrated in Scheme S1. Furthermore, the FFT image at the junction region (inset of Figure 2d) also supports the formation of the epitaxial $NiCo_2S_4$ film, but there is a 6° angle between $NiCo_2S_4$ (440) and $NiCo_2O_4$ (440) facet. In addition, the high-resolution bright-field and dark-field TEM images (Figure 2e) verify again the atomically sharp transition across the junction in annealed $NiCo_2S_4/NiCo_2O_4/MgO$ samples. Then, we employed STEM-EDS mapping to study the elemental distribution across the $NiCo_2S_4/NiCo_2O_4/MgO$ structure. Even distributions of oxygen, sulfur, and magnesium were observed (Figure 3), along with a smooth and distinguishable sulfur/oxygen interface. This EDS analysis illustrates the ability of this top-down strategy to control thickness at the nanometer scale. The successful transformation from $NiCo_2O_4$ to $NiCo_2S_4$ thin film can also be identified by planar RT measurement on annealed

samples. The RT data (Figure S3) clearly shows $NiCo_2S_4$ is a metallic conductor, while $NiCo_2O_4$ is a well-known semi-conductor. To sum up, a unique top-down strategy has been successfully developed to prepare high-quality epitaxial thin film chalcogenides/oxide junctions with nanometer scale thickness control.

**3.3. Top-Down Anion Exchange Process To Form Freestanding $NiCo_2S_4$ Quasi-Single-Crystal Thin Films.** The versatility of our process can be demonstrated by showing that the ion exchange process can be used to make chalcogenide films as thin as 2 nm or as thick as the entire starting $NiCo_2O_4$ film. For example, ca. 2 nm $NiCo_2S_4$ epitaxial thin films were prepared by controlling the anion-exchange time, as shown in Figure S4. In contrast, we have also carried out the anion exchange process to completely consume the $NiCo_2O_4$ film. In the latter case, the complete conversion allows us to easily peel off the $NiCo_2S_4$ film from the MgO substrate due to the huge lattice mismatch, as illustrated in the Scheme S2. These unique freestanding chalcogenide films can
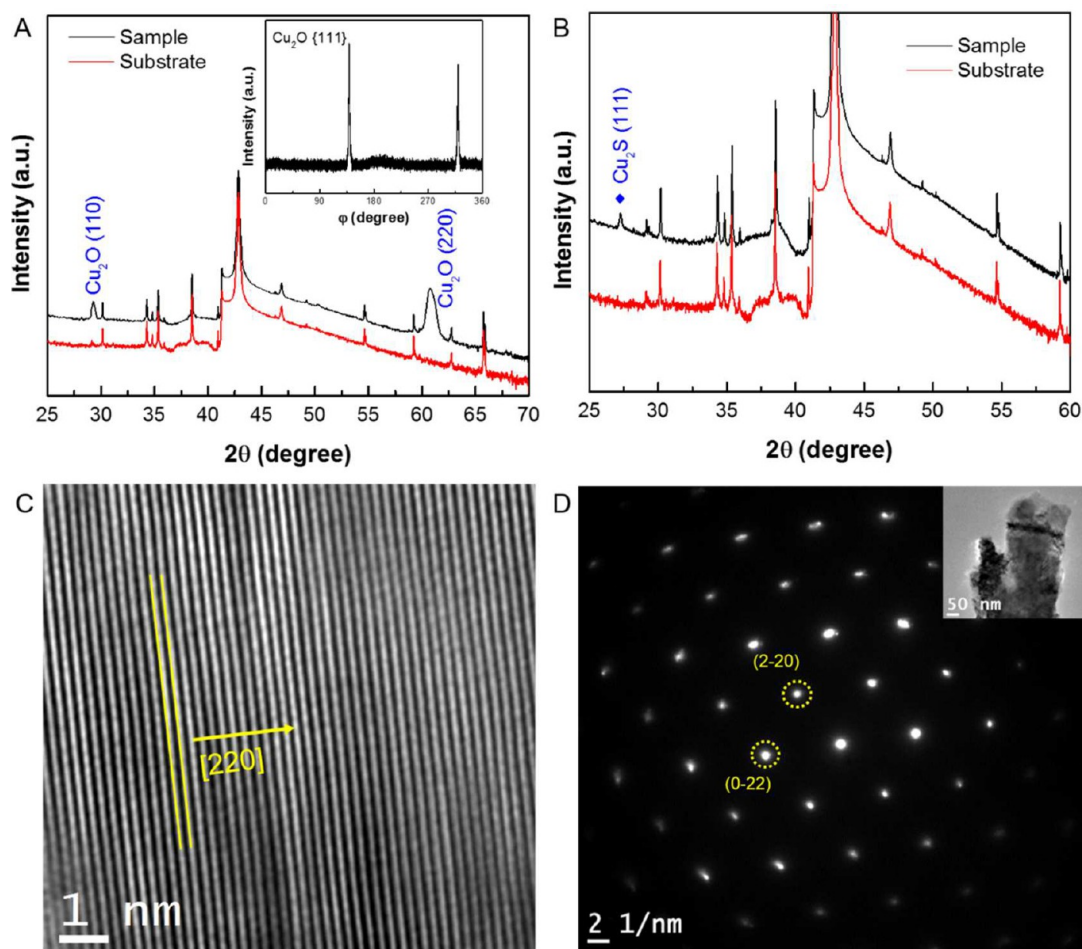
**Figure 6.** Characterization of epitaxial $Cu_2O$ thin films and single-crystal thin $Cu_{1.8}S$ film. The $\theta-2\theta$ XRD pattern of (A) as-prepared $Cu_2O$ and (B) annealed $Cu_{1.8}S$. (JCDPS no. 05-0667 and 24-0061 for $Cu_2O$ and $Cu_{1.8}S$, respectively). The inset of part a shows the phi scan of epitaxial $Cu_2O$ films around their (111) reflections. (C) High-resolution bright-filed TEM image of annealed $Cu_{1.8}S$ thin film. (D) The SAED pattern of annealed single-crystal $Cu_{1.8}S$ thin film collected from the inset of part d.

be transferred onto other substrates for fabrication of functional nanodevices. From the literature survey, we found out that there was a debate in the community about the electrical transport behavior of $NiCo_2S_4$. Is it really a semiconductor with band gap from 1.2−1.7 eV or a metal?[26−28] To help answer this question, an ca. 15 nm-thick freestanding quasi-single-crystal $NiCo_2S_4$ thin film was prepared and transferred onto the Si/$SiO_2$ substrate to study its transport behavior. As shown in Figure 4a, a highly (220) oriented stand-alone thin $NiCo_2S_4$ film is observed, implying a high quality. The inset of Figure 4a shows the HAADF TEM image of a small piece of free-standing $NiCo_2S_4$ thin film. The corresponding SAED of the thin film in Figure 4a is shown in Figure 4b. The quasi-single-crystal nature of the free-standing $NiCo_2S_4$ thin film is revealed by the diffraction dot pattern instead of diffraction circles in Figure 4b. The matched lattice spacing of (400) and (220) facets further supports the formation of thiospinel $NiCo_2S_4$. Details of the device fabrication by e-beam lithography are outlined in the experimental section, and an optical microscope image is shown in Figure 4c. The $RT$ plot of the quasi-single-crystal $NiCo_2S_4$ thin film is shown in Figure 4d. It can be seen that the resistivity of $NiCo_2S_4$ increases linearly with temperature between 2 and 300 K. This positive slope of the $RT$ curve, i.e., $dR/dT > 0$, confirms the metallic behavior and shows that electron−phonon scattering dominates in $NiCo_2S_4$. The Hall

resistivity of the $NiCo_2S_4$ freestanding thin film is presented in Figure 4e. The negative slope of the Hall resistivity vs magnetic field indicates that the electrical transport in $NiCo_2S_4$ is dominated by electrons instead of holes. The calculated carrier density at 2 K is $4.3 \times 10^{22}$ $cm^{-3}$, and the calculated Hall mobility is 23 $cm^2$ $V^{-1}$ $s^{-1}$. This electron mobility of our freestanding $NiCo_2S_4$ thin film is 115 times higher than that obtained from the bulk pellets of the same material,[26] which indicates the high-quality of chalcogenide thin films prepared by our top-down ion exchange process.

**3.4. Top-Down Anion Exchange Process To Form the Lateral $NiCo_2S_4$/$NiCo_2O_4$ Schottky Diode.** Schottky diodes are an important circuit component in many systems. To demonstrate the versatility of our top-down ion exchange process, lateral schottky diodes were fabricated through photolithography and selective anion-exchange process performed on $NiCo_2O_4$ epitaxial thin film, as shown in the schematic in Figure 5a (see details in the Experimental Section). Figure 5b shows an optical microscope image of the interface between the $NiCo_2O_4$ film and the region which was selectively converted to $NiCo_2S_4$. The image shows that we have formed a $NiCo_2S_4$/$NiCo_2O_4$ heterojunction with well-defined interface. The current−voltage ($I−V$) characteristics of the $NiCo_2S_4$/$NiCo_2O_4$ heterojunction were measured and are shown in Figure 4b. The $I−V$ curves in Figure 4c clearly show

that the $NiCo_2S_4/NiCo_2O_4$ heterojunction exhibits reversible, rectifying behavior, where current is amplified significantly when metallic $NiCo_2S_4$ is positively biased. From the $I-V$ plot, we estimate the turn-on voltage to be about 0.5 V under forward bias. The $I-V$ curves were repeatedly measured in both directions (forward scan and reverse scan), and we find that the $I-V$ curves nearly coincide, irrespective of the voltage scan direction. To confirm that the $I-V$ characteristics in Figure 5c are in fact due to the $NiCo_2S_4/NiCo_2O_4$ junction itself, the $I-V$ characteristics between Al-$NiCo_2S_4$ and Al-$NiCo_2O_4$ were carefully checked. The linear $I-V$ curve in Figure 5d demonstrates that Ohmic contact exists between metal Al and metallic $NiCo_2S_4$. Similarly, the nearly symmetric and weak nonlinear $I-V$ curve in Figure 5e demonstrate no barriers between metal Al and semiconducting $NiCo_2O_4$. These results confirm that we have successfully formed a lateral Schottky diode between $NiCo_2O_4$ and $NiCo_2S_4$ by our selective anion-exchange process.

**3.5. Top-Down Anion Exchange Process To Form $Cu_{1.8}S$ Quasi-Single-Crystal Thin Films.** To further assess the generality of this top-down approach, we tested the ion-exchange process in making semiconductor chalcogenide thin films. Specifically, we synthesized high-quality $Cu_{1.8}S$ thin films using a similar strategy. We first prepared epitaxial $Cu_2O$ thin film on MgO (001) substrate as template using reactive sputtering (see the Experimental Section for details). As shown in Figure 6a, the $\theta-2\theta$ XRD pattern of the $Cu_2O$ thin film clearly shows the strong peaks of (110) and (220) reflections, suggesting the high crystalline quality of the film with [110] orientation. Further, we conducted the XRD $\varphi$ scan around $Cu_2O$ (111) reflections on the as-obtained thin films. The 2-fold symmetry (inset of Figure 6a) from $Cu_2O$ (111) confirms the (110) oriented epitaxial growth of $Cu_2O$ on the MgO substrate. Next, the epitaxial $Cu_2O$ thin films were used as precursor to form high-quality copper sulfide thin films. After anion-exchange and postannealing treatment, the orange $Cu_2O$ thin films turned brown, indicating the formation of copper sulfide. The XRD $\theta-2\theta$ scan of the sulfide films shows only one distinguishable peak at 27.4°, which matches the $Cu_{1.8}S$ (111) reflection, suggesting the formation of highly oriented thin films. To further demonstrate the high-quality of the $Cu_{1.8}S$ thin films, TEM studies were employed, as shown in the high-resolution TEM analysis in Figure 6. The resolved lattice fringes in Figure 6c give an interplanar spacing of ca. 0.198 nm, which corresponds to the $Cu_{1.8}S$ (220) planes. We further conducted SAED studies on the $Cu_{1.8}S$ thin films (inset of Figure 6d). The single-crystal nature of the $Cu_{1.8}S$ thin films is indeed confirmed by the electron diffraction pattern (Figure 6d). Interestingly, our electrical transport data show that the as-prepared $Cu_{1.8}S$ thin films exhibit p-type semiconducting behavior (Figure S5). The room-temperature carrier density and mobility of these films are $2.7 \times 10^{20}$ $cm^{-3}$ and 16.02 $cm^2$ $V^{-1}$ $s^{-1}$, respectively. In addition, the room-temperature mobility of the $Cu_{1.8}S$ thin films made by our ion exchange process is very close to that of the p-type single-crystal copper sulfide sample (25 $cm^2$ $V^{-1}$ $s^{-1}$),[29] which is much higher than previously reported for the $Cu_{1.8}S$ thin film (0.58 $cm^2$ $V^{-1}$ $s^{-1}$).[30] Thus, the electrical transport measurements confirm the high quality of epitaxial $Cu_{1.8}S$ thin films made by our top down ion exchange process.

## 4. CONCLUSIONS

In general, we have successfully demonstrated a simple top-down ion-exchange process to fabricate high quality chalcogenide thin films with nanometer scale thickness control. The process was used to produce epitaxial metallic ($NiCo_2S_4$) and semiconducting ($Cu_{1.8}S$) chalcogenide films on single crystal substrates. Unlike bottom-up approaches, this process was successfully used to produce epitaxial free-standing chalcogenide films and to form *in situ* atomically flat junctions, including functional Schottky diodes. The advantage of our top-down approach is reflected in the excellent properties of the chalcogenide thin films we have prepared. For example, we measured mobility of 23 $cm^2$ $V^{-1}$ $s^{-1}$ for $NiCo_2S_4$ and 16.02 $cm^2$ $V^{-1}$ $s^{-1}$ for $Cu_{1.8}S$ thin films, which are substantially higher than other solution-prepared samples (0.2 $cm^2$ $V^{-1}$ $s^{-1}$ for $NiCo_2S_4$; 0.58 $cm^2$ $V^{-1}$ $s^{-1}$ for $Cu_{1.8}S$), confirming the potential of our technique for synthesis of high-quality chalcogenide thin films. This approach has far-reaching implications for a wide range of applications in energy and electronics.

## ■ ASSOCIATED CONTENT

### Ⓢ Supporting Information

The Supporting Information is available free of charge on the ACS Publications website at DOI: 10.1021/acs.chemmater.6b04319.

Additional crystal transformation schemes and characterization data (PDF)

## ■ AUTHOR INFORMATION

### Corresponding Authors
*(H.N.A.) E-mail: alshareef@kaust.edu.sa.
*(X.Z.) E-mail: xixiang.zhang@kaust.edu.sa.
### ORCID Ⓞ
Husam N. Alshareef: 0000-0001-5029-2142
### Author Contributions
†C.X. and P.L. contributed equally.
### Notes
The authors declare no competing financial interest.

## ■ ACKNOWLEDGMENTS

## ■ REFERENCES

(1) Frumar, M.; Frumarova, B.; Nemec, P.; Wagner, T.; Jedelsky, J.; Hrdlicka, M. Thin chalcogenide films prepared by pulsed laser deposition−new amorphous materials applicable in optoelectronics and chemical sensors. *J. Non-Cryst. Solids* **2006**, *352*, 544−561.

(2) Andriesh, A.; Iovu, M.; Shutov, S. Chalcogenide non-crystalline semiconductors in optoelectronics. *J. Optoelectron. Adv. Mater.* **2002**, *4*, 631−647.

(3) Scheer, R.; Schock, H.-W. *Chalcogenide Photovoltaics: Physics, Technologies, and Thin Film Devices*; John Wiley & Sons: 2011.

(4) Green, M. A. Thin-film solar cells: review of materials, technologies and commercial status. *J. Mater. Sci.: Mater. Electron.* **2007**, *18*, 15−19.

(5) Anwar, S.; Gowthamaraju, S.; Mishra, B.; Singh, S.; Anwar, S. Spray pyrolysis deposited tin selenide thin films for thermoelectric applications. *Mater. Chem. Phys.* **2015**, *153*, 236−242.

(6) Kim, D.-H.; Byon, E.; Lee, G.-H.; Cho, S. Effect of deposition temperature on the structural and thermoelectric properties of bismuth telluride thin films grown by co-sputtering. *Thin Solid Films* **2006**, *510*, 148−153.

(7) Mourzina, Y. G.; Schubert, J.; Zander, W.; Legin, A.; Vlasov, Y. G.; Lüth, H.; Schöning, M. J. Development of multisensor systems based on chalcogenide thin film chemical sensors for the simultaneous multicomponent analysis of metal ions in complex solutions. *Electrochim. Acta* **2001**, *47*, 251−258.

(8) Mourzina, Y.; Yoshinobu, T.; Schubert, J.; Lüth, H.; Iwasaki, H.; Schöning, M. J. Ion-selective light-addressable potentiometric sensor (LAPS) with chalcogenide thin film prepared by pulsed laser deposition. *Sens. Actuators, B* **2001**, *80*, 136−140.

(9) Yue, R.; Barton, A. T.; Zhu, H.; Azcatl, A.; Pena, L. F.; Wang, J.; Peng, X.; Lu, N.; Cheng, L.; Addou, R.; et al. HfSe2 thin films: 2D transition metal dichalcogenides grown by molecular beam epitaxy. *ACS Nano* **2015**, *9*, 474−480.

(10) Verger, F.; Nazabal, V.; Colas, F.; Němec, P.; Cardinaud, C.; Baudet, E.; Chahal, R.; Rinnert, E.; Boukerma, K.; Péron, I.; et al. RF sputtered amorphous chalcogenide thin films for surface enhanced infrared absorption spectroscopy. *Opt. Mater. Express* **2013**, *3*, 2112−2131.

(11) Mane, R.; Lokhande, C. Chemical deposition method for metal chalcogenide thin films. *Mater. Chem. Phys.* **2000**, *65*, 1−31.

(12) Vanalakar, S.; Agawane, G.; Kamble, A.; Hong, C.; Patil, P.; Kim, J. Fabrication of Cu 2 SnS 3 thin film solar cells using pulsed laser deposition technique. *Sol. Energy Mater. Sol. Cells* **2015**, *138*, 1−8.

(13) Yao, T.; Takeda, T. Growth process in atomic layer epitaxy of Zn chalcogenide single crystalline films on (100) GaAs. *Appl. Phys. Lett.* **1986**, *48*, 160−162.

(14) Luo, H. M.; Lin, Y.; Wang, H. Y.; Lee, J. H.; Suvorova, N. A.; Mueller, A. H.; Burrell, A. K.; McCleskey, T. M.; Bauer, E.; Usov, I. O.; Hawley, M. E.; Holesinger, T. G.; Jia, Q. X. A Chemical Solution Approach to Epitaxial Metal Nitride Thin Films. *Adv. Mater.* **2009**, *21*, 193−197.

(15) Duan, X.; Wang, C.; Shaw, J. C.; Cheng, R.; Chen, Y.; Li, H.; Wu, X.; Tang, Y.; Zhang, Q.; Pan, A.; et al. Lateral epitaxial growth of two-dimensional layered semiconductor heterojunctions. *Nat. Nanotechnol.* **2014**, *9*, 1024−1030.

(16) Pospischil, A.; Furchi, M. M.; Mueller, T. Solar-energy conversion and light emission in an atomic monolayer pn diode. *Nat. Nanotechnol.* **2014**, *9*, 257−261.

(17) Powell, A. E.; Hodges, J. M.; Schaak, R. E. Preserving Both Anion and Cation Sublattice Features during a Nanocrystal Cation Exchange Reaction: Synthesis of Metastable Wurtzite-Type CoS and MnS. *J. Am. Chem. Soc.* **2016**, *138*, 471−474.

(18) Son, D. H.; Hughes, S. M.; Yin, Y.; Alivisatos, A. P. Cation exchange reactions in ionic nanocrystals. *Science* **2004**, *306*, 1009−1012.

(19) Wu, H.-L.; Sato, R.; Yamaguchi, A.; Kimura, M.; Haruta, M.; Kurata, H.; Teranishi, T. Formation of pseudomorphic nanocages from Cu2O nanocrystals through anion exchange reactions. *Science* **2016**, *351*, 1306−1310.

(20) Hodges, J. M.; Kletetschka, K.; Fenton, J. L.; Read, C. G.; Schaak, R. E. Sequential Anion and Cation Exchange Reactions for Complete Material Transformations of Nanoparticles with Morphological Retention. *Angew. Chem.* **2015**, *127*, 8793−8796.

(21) Rivest, J. B.; Buonsanti, R.; Pick, T. E.; Zhu, L.; Lim, E.; Clavero, C.; Schaible, E.; Helms, B. A.; Milliron, D. J. Evolution of Ordered Metal Chalcogenide Architectures through Chemical Transformations. *J. Am. Chem. Soc.* **2013**, *135*, 7446−7449.

(22) Bitla, Y.; Chin, Y.-Y.; Lin, J.-C.; Van, C. N.; Liu, R.; Zhu, Y.; Liu, H.-J.; Zhan, Q.; Lin, H.-J.; Chen, C.-T.; et al. Origin of metallic behavior in NiCo2O4 ferrimagnet. *Sci. Rep.* **2015**, *5*, 15201.

(23) Krivanek, O. L.; Chisholm, M. F.; Nicolosi, V.; Pennycook, T. J.; Corbin, G. J.; Dellby, N.; Murfitt, M. F.; Szilagyi, Z. S.; Oxley, M. P.; Pantelides, S. T. Atom-by-atom structural and chemical analysis by annular dark-field electron microscopy. *Nature* **2010**, *464*, 571−574.

(24) Hu, L.; Wu, L.; Liao, M.; Hu, X.; Fang, X. Electrical transport properties of large, individual NiCo2O4 nanoplates. *Adv. Funct. Mater.* **2012**, *22*, 998−1004.

(25) Silwal, P.; Miao, L.; Stern, I.; Zhou, X.; Hu, J.; Kim, D. H. Metal insulator transition with ferrimagnetic order in epitaxial thin films of spinel NiCo2O4. *Appl. Phys. Lett.* **2012**, *100*, 032102.

(26) Xia, C.; Li, P.; Gandi, A. N.; Schwingenschlögl, U.; Alshareef, H. N. Is NiCo2S4 really a semiconductor? *Chem. Mater.* **2015**, *27*, 6482−6485.

(27) Chen, H.; Jiang, J.; Zhang, L.; Wan, H.; Qi, T.; Xia, D. Highly conductive NiCo 2 S 4 urchin-like nanostructures for high-rate pseudocapacitors. *Nanoscale* **2013**, *5*, 8879−8883.

(28) Du, W.; Zhu, Z.; Wang, Y.; Liu, J.; Yang, W.; Qian, X.; Pang, H. One-step synthesis of CoNi 2 S 4 nanoparticles for supercapacitor electrodes. *RSC Adv.* **2014**, *4*, 6998−7002.

(29) Abdullaev, G.; Aliyarova, Z.; Zamanova, E.; Asadov, G. Investigation of the electric properties of Cu2S single crystals. *Phys. Status Solidi B* **1968**, *26*, 65−68.

(30) Bhattacharya, R.; Pramanik, P. New chemical methods for the deposition of Cu1· 8S and TlSe thin film. *Bull. Mater. Sci.* **1981**, *3*, 403−408.